

Structure and stability of the neurotoxin PV2 from the eggs of the apple snail *Pomacea canaliculata*

María Victoria Frassa^a, Marcelo Ceolín^a, Marcos S. Dreón^b, Horacio Heras^{b,c,*}

^a Instituto de Investigaciones Físico-Químicas, Teóricas y Aplicadas (INIFTA), Universidad Nacional de La Plata - CONICET CCT-La Plata, Argentina

^b Instituto de Investigaciones Bioquímicas de La Plata (INIBIOLP), Universidad Nacional de La Plata - CONICET CCT-La Plata, Argentina

^c Cátedra de Química Biológica, Facultad de Ciencias Naturales y Museo, UNLP, La Plata, Argentina

A B S T R A C T

There is little information on the egg proteins of gastropod mollusks. Here we focus on PV2, a novel neurotoxin from snail eggs, studying its size, shape, structure, and stability, using small angle X-ray scattering (SAXS), absorption and fluorescence spectroscopy, circular dichroism, electron microscopy and partial proteolysis. Results indicate that PV2 is a compact and well folded oligomer of 130×44 Å. It is an octamer of four 98 kDa heterodimers composed of 67 and 31 kDa subunits. Subunits are held together by disulfide bonds. Dimers are assembled into native PV2 by non-covalent forces. The larger subunit is more susceptible to proteolysis, indicating it is less compactly folded and/or more exposed. Quenching of tryptophan fluorescence showed a single class of tryptophyl side chains occluded in hydrophobic regions. Native structure shows loss of secondary structure ($\alpha + \beta$) at 6 M urea or 60–70 °C; the effects on the quaternary structure suggest an unfolding without disassembling of the protein. The 3D model of PV2 presented here is the first for an egg proteinaceous neurotoxin in animals.

Keywords:

Neurotoxin
Perivitellin
3D structure
Protein stability
Quaternary protein structure
Snail
Mollusc

1. Introduction

Pomacea canaliculata (golden apple snail) is a freshwater snail native to the Amazon and Plata basins, where its seasonal reproduction is mostly affected by changes in environmental temperatures and the availability of water [1–3]. Among their adaptations is the strategy to deposit its eggs above the waterline on vegetation and rocks in a calcareous and brightly colored clutch probably warning predators of its defenses (Fig. 1S). This remarkable egg-laying strategy exposes the eggs to high temperatures, desiccation and terrestrial predators. Moreover, many eggs are laid on rocks, directly exposed to the sun for several hours a day and still hatch normally, suggesting biochemical adaptations providing protection against thermal stress and desiccation. Among the adaptations to cope with this harsh environment is the provision of eggs with a perivitellin fluid surrounding embryos that acts as its main nutrition and protection source [4,5]. Those Ampullariid species with aerial eggs clutches have the perivitellin fluid mostly composed of polysaccharides and glyco-lipo-carotenoproteins complexes called perivitellins [6,7]. In particular, the major

perivitellins found in *P. canaliculata* are ovorubin, PV2 and PV3, oligomeric proteins that are emerging as a very efficient and complex protection and defense system for the developing embryos. Previous studies have focused on ovorubin, the most abundant carotenoprotein, with multiple functions and remarkable structural characteristics such as a thermal stability higher than 95 °C [8–11]. A perivitellin named scalarin, with similar functions and structural features was isolated from *Pomacea scalaris*, a related snail species [12]. PV2 is the other major egg protein of *P. canaliculata* with an apparent MW of 400 kDa. It is composed of two subunits of 67 kDa (Swiss-Prot accession no. **POC8G6**) and 31 kDa (Swiss-Prot accession no. **POC8G7**). It is a very high-density glycolipoprotein (VHDL) with 3.7% lipids and 2.5% carbohydrates [6]. As part of the egg perivitellin fluid, it carries out a number of activities – structural, dietary and protective – before being incorporated and degraded by the embryo during development [4]. Recently we have uncovered its neurotoxic nature, a novel and unusual role for an animal egg protein [13] commented in Swiss-Prot protein monthly review spotlight [14]. PV2 is biochemically and functionally well characterized, but structural information is lacking. In fact, except for the detailed studies on ovorubin, there is little information on the structure and stability of this interesting group of egg proteins in invertebrates.

In this work, we report PV2 structural features, dimensions and global shape as well as its changes induced by temperature and chaotropic agents, studied by means of small angle X-ray scattering (SAXS), absorption and fluorescence spectroscopy, circular dichroism

(CD), transmission electron microscopy (TEM) and partial proteolysis with a view to shed light into the structure–function relationships and the physiological meaning in embryogenesis.

2. Experimental procedures

2.1. Eggs

Eggs of *P. canaliculata* were collected in ponds near La Plata, province of Buenos Aires, Argentina between October and April (reproductive season). Only egg masses having embryos developed to no more than the morula stage were used. Voucher specimens collected in the same location were deposited in the Museum of La Plata collection (MLP 12936) for further reference.

2.2. PV2 isolation and purification

Eggs were rinsed with ice cold 20 mM Tris/HCl, pH 6.8 buffer, containing a protease inhibitor cocktail (Sigma Chemicals, St. Louis) using a Potter type homogenizer (Thomas Sci., Swedesboro). The buffer: sample ratio was kept at 3:1. The crude homogenate was centrifuged sequentially at 10,000×g for 30 min and at 100,000×g for 50 min. The pellet was discarded and the supernatant was layered on NaBr $\delta = 1.28$ g/mL and ultracentrifuged at 207,000×g for 22 h, at 10 °C on a Beckman L8M with a swinging bucket rotor SW 60.Ti (Beckman, Palo Alto).

Aliquots with PV2 fraction were pooled, desalted and concentrated using Centricon membrane concentrators with a MW 50,000 cut off (Amicon, Beverly, MA).

The soluble protein fraction obtained using the above procedure was purified in a Merck-Hitachi high performance liquid chromatograph (HPLC) (Hitachi Ltd., Tokyo, Japan) with an L-6200 Intelligent Pump and an L-4200 UV detector set at 280 nm. The sample was analyzed in a Mono Q HR 10/10 (Amersham-Pharmacia, Uppsala, Sweden) using a gradient of 0–1 M NaCl in a 20 mM Tris buffer.

Protein content was determined by the method of Lowry [15] using Bovine Serum Albumin (BSA) as standard.

Purity was checked by native PAGE in 4–20% gradient polyacrylamide gels using a Mini-Protean III System (Bio Rad Laboratories, Inc., Hercules, CA), and high molecular weight standards (Pharmacia) were run in the same gels and were stained with Coomassie Brilliant Blue R-250 (Sigma).

2.3. Absorption spectroscopy

UV–Vis spectra of PV2 were made in a Jasco 550 spectrophotometer. Samples were measured at a concentration of 1.2 μ M in buffer Pi 20 mM NaCl. Spectral scanning was performed at 40 nm/min scan speed, 1 nm bandwidth. The spectrum was obtained averaging 10 individual runs. Appropriate buffer spectra were subtracted from raw data. In order to obtain the fourth-derivative signal of the spectrum, the data were smoothed twice using an adjacent-averaging algorithm (5-point window) [16] before each derivative calculation [17].

2.4. Proteinase K treatment and electrophoresis

Native PV2 was subjected to enzymatic digestion with proteinase K (Promega) supplied as lyophilized powder and reconstituted in 50 mM Tris–HCl pH 8.0 10 mM CaCl₂. PV2 (1 mg/mL) was incubated with proteinase K (1; 10 and 100 μ g/mL) at 37 °C for 30 min. Digestion was terminated by boiling samples in SDS sample buffer with β -mercaptoethanol and digestion products analyzed on a 4–20% SDS-PAGE.

Samples of PV2 with and without β -mercaptoethanol treatment were analyzed on (4–20%) SDS-PAGE to determine if intercatenary

disulfide bonds were involved in the maintenance of the protein structure [18].

2.5. Fluorescence spectroscopy

Fluorescence spectra of PV2 (1.2 μ M) were recorded in scanning mode in an Olis-upgraded SLM 4800 (Bogart, GA). Tryptophan emission was excited at 270 nm (4 nm slit) and recorded between 310 and 410 nm (4 nm slit) unless otherwise indicated. All the experiments were performed in 20 mM phosphate buffer, pH 7.0 (buffer Pi) supplemented with 50 mM NaCl. Fluorescence measurements were performed in 5 mm optical-path-length quartz-cells at different urea and temperature values according to the experiments.

Acrylamide quenching experiments were performed to assess the solvent accessibility of tryptophan residues. Successive aliquots of acrylamide (1.5 M stock solutions in buffer Pi) were added to a 1.2 μ M protein solution (starting concentration) in order to reach up to 1 M quencher concentration. Tryptophan was excited at 280 nm (4 nm slit) and emission recorded between 305 and 445 nm (4 nm slit). Data were corrected for protein dilution.

Cysteine quantification was performed by monitoring the fluorescence emission of the dye monobromobimane (mBrB, Fluka) following the procedure of Kosower and Kosower [19]. Briefly, 10 μ L of an acetonitrile solution of 100 μ M mBrB was added to 520 μ L of a PV2 solution in phosphate buffer 20 mM pH 7.2, and different urea concentrations to achieve a final concentration of 0.025 μ M PV2, 1.88 μ M mBrB. The number of dye-exposed cysteines was determined comparing the fluorescence signal with the emission obtained from a control BSA solution (0.025 μ M in 8 M urea, Pi 20 mM, pH 7.2). Samples were incubated overnight before fluorescence recording.

2.6. Circular dichroism spectroscopy

Far Circular Dichroism (fCD) spectra (190–240 nm) and Near Circular Dichroism (nCD) spectra (260–320 nm) were recorded with a Jasco J-810 spectropolarimeter (0.5 nm bandwidth, 100 nm min⁻¹, 4 s average time, 3 spectra average) using 0.1 mm (fCD) or 1 cm (nCD) quartz cells placed in a thermostated cell holder at 20 °C. PV2 was dissolved in 20 mM phosphate buffer pH 7.4 at 0.15 μ M (fCD) or 1.2 μ M (nCD). Buffer ellipticity was subtracted from each individual spectrum.

CD melting experiments were performed by monitoring the CD signal at 222 nm during temperature scanning at 2 °C min⁻¹ using a Peltier heating element.

Secondary structure content was estimated through analysis of the molar ellipticities with the K2d [20] and Contin algorithms [21].

2.7. Small angle X-ray scattering (SAXS)

SAXS experiments were performed at the D02A-SAXS2 line operating in the Laboratorio Nacional Luz Síncrotron, Campinas (SP, Brazil). The scattering pattern was detected using a MARCCD bidimensional charge coupled device assisted by FIT 2D software (<http://www.esrf.fr/computing/scientific/FIT2D>). The sample cell was built using two parallel mica windows 1 mm apart leaving 300 μ L free volume for the sample. The wavelength used was 1.448 Å and the sample was at 1044 mm from to the detector allowing a nominal Q-range between 0.012 and 0.25 Å⁻¹ (nominal $D_{\max} \leq 260$ Å). The temperature was controlled using a circulating-water bath and samples were heated stepwise from 20 to 70 °C. Sample temperature was monitored using a thermocouple device attached directly to the sample cell.

Corrections of beam intensity, detector homogeneity and sample absorption were performed following standard procedures. At least 3 independent curves were averaged for each single experiment. The size of PV2 was determined using the gyration radii (R_G) obtained by

analysis of SAXS patterns as Guinier plots ($\ln(I) = \ln(I_0) - R_G Q^2/3$, $Q = 4\pi \sin(\theta)/\lambda$, $R_G Q \leq 1$) and the globularity evaluated by inspecting the Kratky plot ($I(Q) \cdot Q^2$ vs. Q). The low-resolution shape model of PV2 was obtained from the algorithm built in the program DAMMIN 5.3 [22]. Briefly, DAMMIN uses simulated annealing optimization to generate a bead model giving the best fit to the scattering data. Pair-distance distribution function ($P(r)$) obtained from scattering data was calculated using Regularized Fourier Transform built in the program GNOM 4.5 [23]. The resulting dummy atom model represents the shape of the scattering particle. To increase the reliability of the results, the final model was obtained by means of a spatial average of 16 independent low-resolution models calculated with the package program DAMAVER [24].

2.8. Transmission electron microscopy

Samples for transmission electron microscopy (TEM) of native PV2 5 μM in buffer Pi were stained with 1% (w/v) sodium phosphotungstate, pH 7.4, blotted and air-dried. Images were recorded under low-dose conditions in a JEM-1200 EX transmission electron microscope (Tokyo, Japan). Statistical analysis of the particle size distribution was carried out using the tools built in the program ImageJ 1.36b (<http://rsb.info.nih.gov/ij/>).

3. Results

3.1. Size and global shape of PV2

The size and global shape of the quaternary structure of native PV2 were studied by means of SAXS experiments. The data obtained were normalized for protein concentration and depicted in Fig. 1A. A gyration radius of $44 \pm 1 \text{ \AA}$ was obtained from the Guinier plot (inset in Fig. 1A). The Kratky plot has the typical bell-shaped form expected for globular proteins (Fig. 1B). Fig. 1C shows the pair distance distribution $P(r)$ obtained using the regularized Fourier Transform method implemented in the program GNOM 4.5 [25]. The $P(r)$ obtained for native PV2 shows a maximum at 44 \AA with a well defined $D_{\text{max}} = 130 \text{ \AA}$ compatible with an anisometric particle. A low-resolution model for native PV2 was obtained using Simulated Annealing Algorithms implemented in the program DAMMIN [22]. The final model, obtained by averaging 16 independently calculated models using the algorithms implemented in the program package DAMAVER [24], is depicted in Fig. 2. This *ab initio* dummy atom model fitted satisfactorily with the experimental scattering intensity data (Fig. 1C). Image analysis of TEM data helped to obtain the size distribution curve of these particles. The particle size distributions for the protein are shown as a histogram where a maximum around 137 \AA can be observed (Fig. 1D and Fig. 2S).

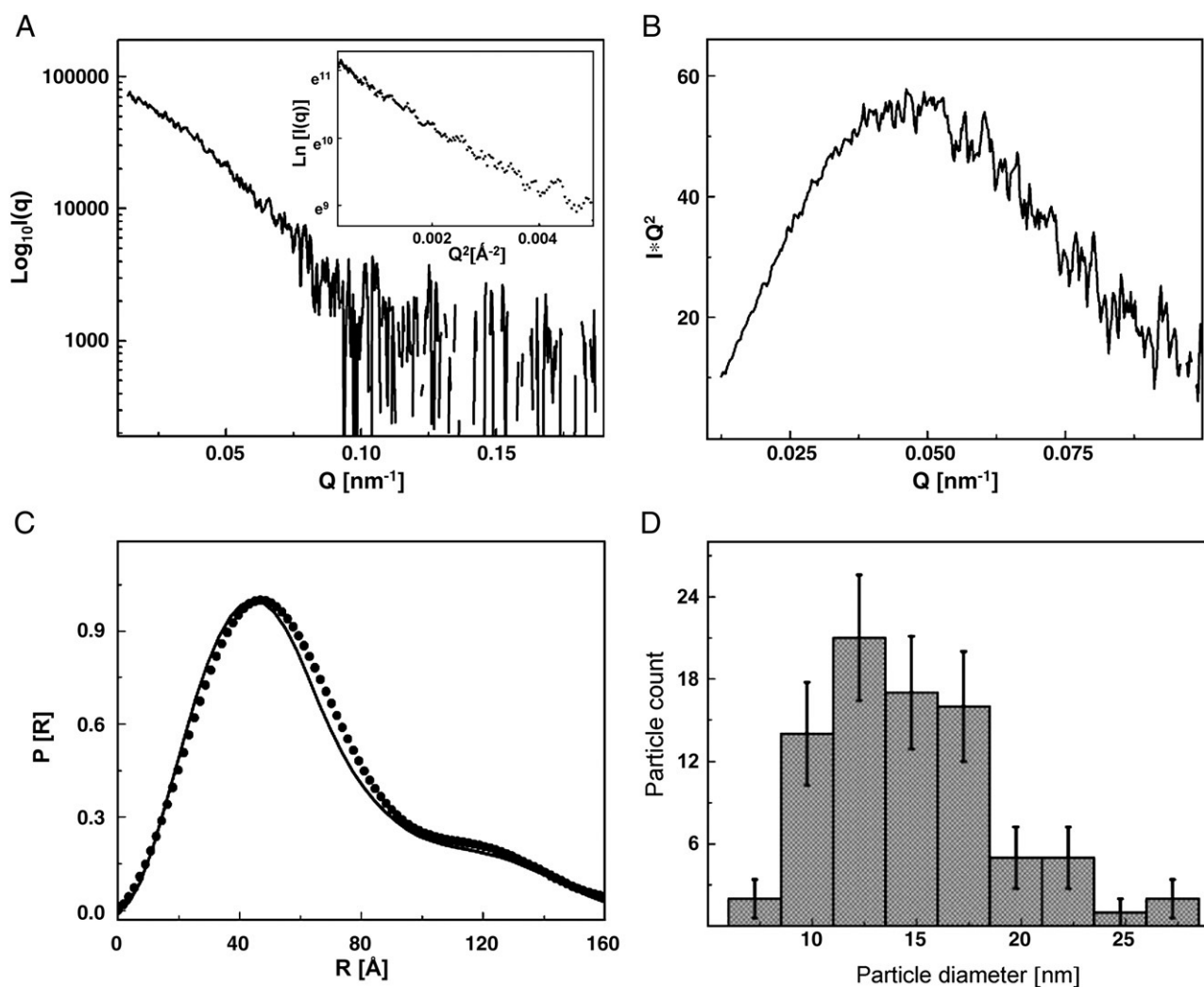


Fig. 1. PV2 solution structure by SAXS. (A) Raw SAXS data. Inset: Guinier region in linearized variables. (B) Kratky plot $[I(Q) \cdot Q^2$ vs. $Q]$ of the data depicted in panel A. (C) Pair-distance distribution obtained from data in panel A using the program GNOM v4.5. Dotted line: Scattering intensity of experimental data for PV2; solid line: Theoretical *ab initio* dummy atom model. See Experimental procedures for details. (D) Size distribution of PV2 molecules obtained by transmission electron microscopy analysis (see Fig. 2S for image).

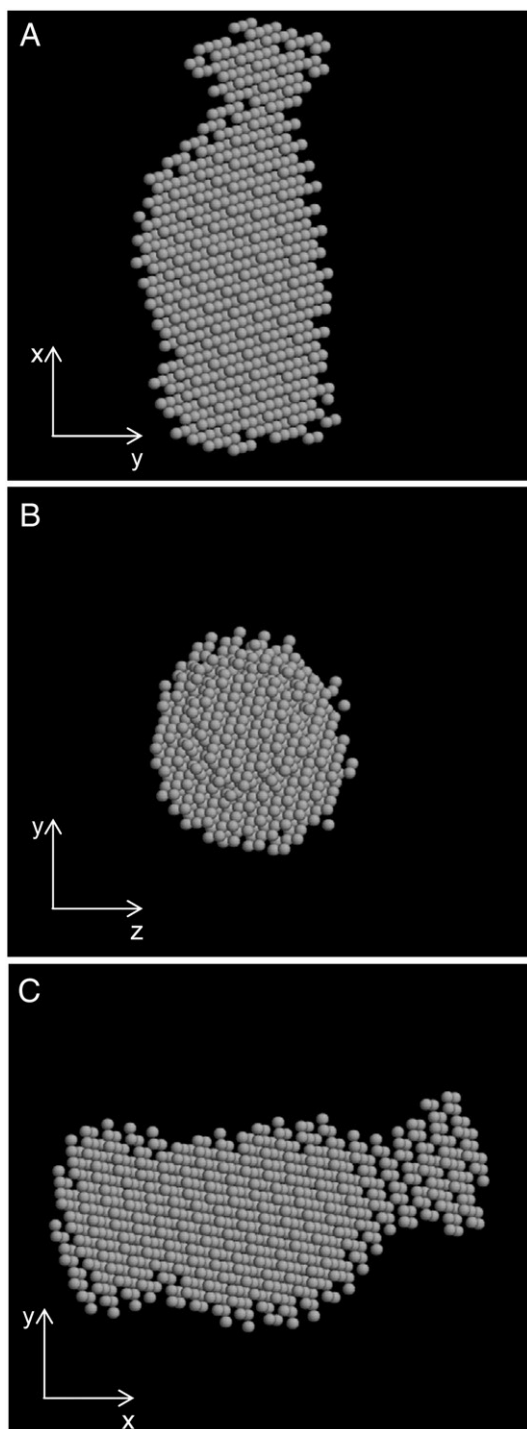


Fig. 2. Three-dimensional shape model of PV2 obtained from SAXS data using the *ab initio* methods implemented in DAMMIN (see Experimental procedures). Referred to (A) view; (B) rotated 90° around y-axis; (C) rotated 90° around z-axis.

3.2. Structural features

The ca. 400 kDa native PV2 is an octamer of 4 identical 98 kDa heterodimers, each composed of one 67 and one 31 kDa subunits. The presence of intercatenary disulfide bonds among PV2 subunits was revealed through SDS-PAGE with and without β -mercaptoethanol. Fig. 4D shows that the 98 kDa heterodimer subunits are held together by disulfide bridges and that these heterodimers are assembled into native PV2 by non-covalent forces.

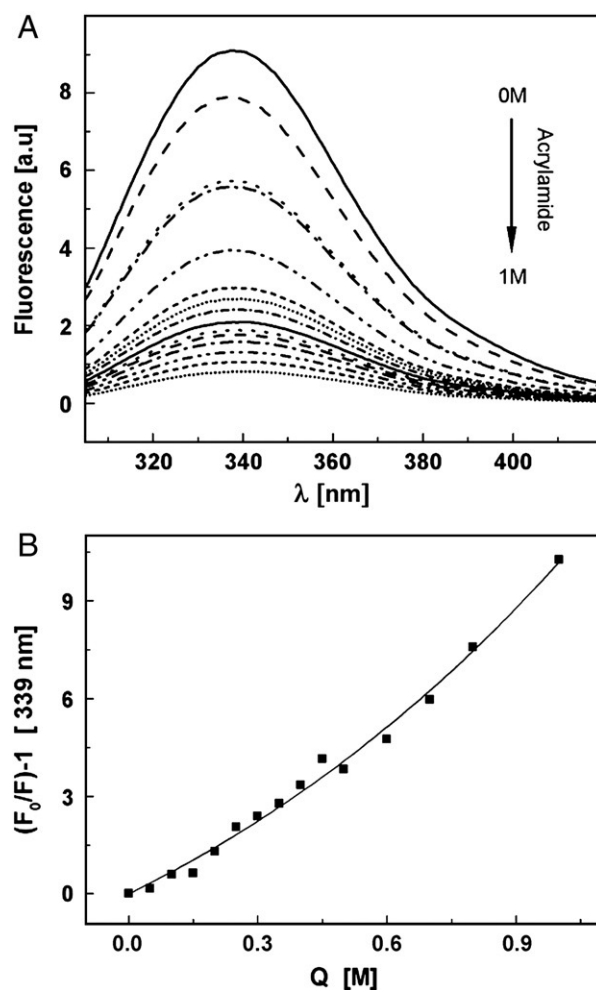


Fig. 3. Quenching of PV2 tryptophan fluorescence spectra by acrylamide. (A) Tryptophan fluorescence spectra obtained by titration of PV2 with acrylamide (0 to 1 M). (B) Stern-Volmer plot obtained from the fluorescence intensity at 339 nm (spectral maximum). Solid line corresponds to the fit of Eq. (1) to the experimental data.

3.3. Proteinase K susceptibility

To analyze the relative exposure of the protein subunits to the aqueous medium, their susceptibilities to limited proteolysis by proteinase K were assayed. Incubation of PV2 with the protease, followed by SDS-PAGE analysis showed extensive degradation of the 67 kDa subunit (Fig. 5). However, the 31 kDa subunit was resistant to cleavage by protease under controlled conditions. This indicates that the 31 kDa subunit is not exposed to the aqueous medium or folded in such a way that it is not susceptible to proteolysis.

3.4. Spectroscopy

The UV absorption spectrum of native PV2, together with its fourth derivative spectrum is shown in Fig. 4A. It is clearly dominated by strong signals arising from Trp (290 nm) and Phe (260 nm), respectively. The fluorescence emission spectrum of the protein is shown in Fig. 4B where a maximum at 338 nm suggests that Trp indole rings are placed in a hydrophobic environment, also indicated by CD and the acrylamide fluorescence quenching experiments (see below). The fCD and nCD spectra obtained for native PV2 are depicted in Fig. 4C. Both the K2D algorithm [20] and CONTIN algorithm [21] applied to the fCD data gave consistent results estimating an average of 21% α structure, 25% β structure and 54% random coil or unstructured

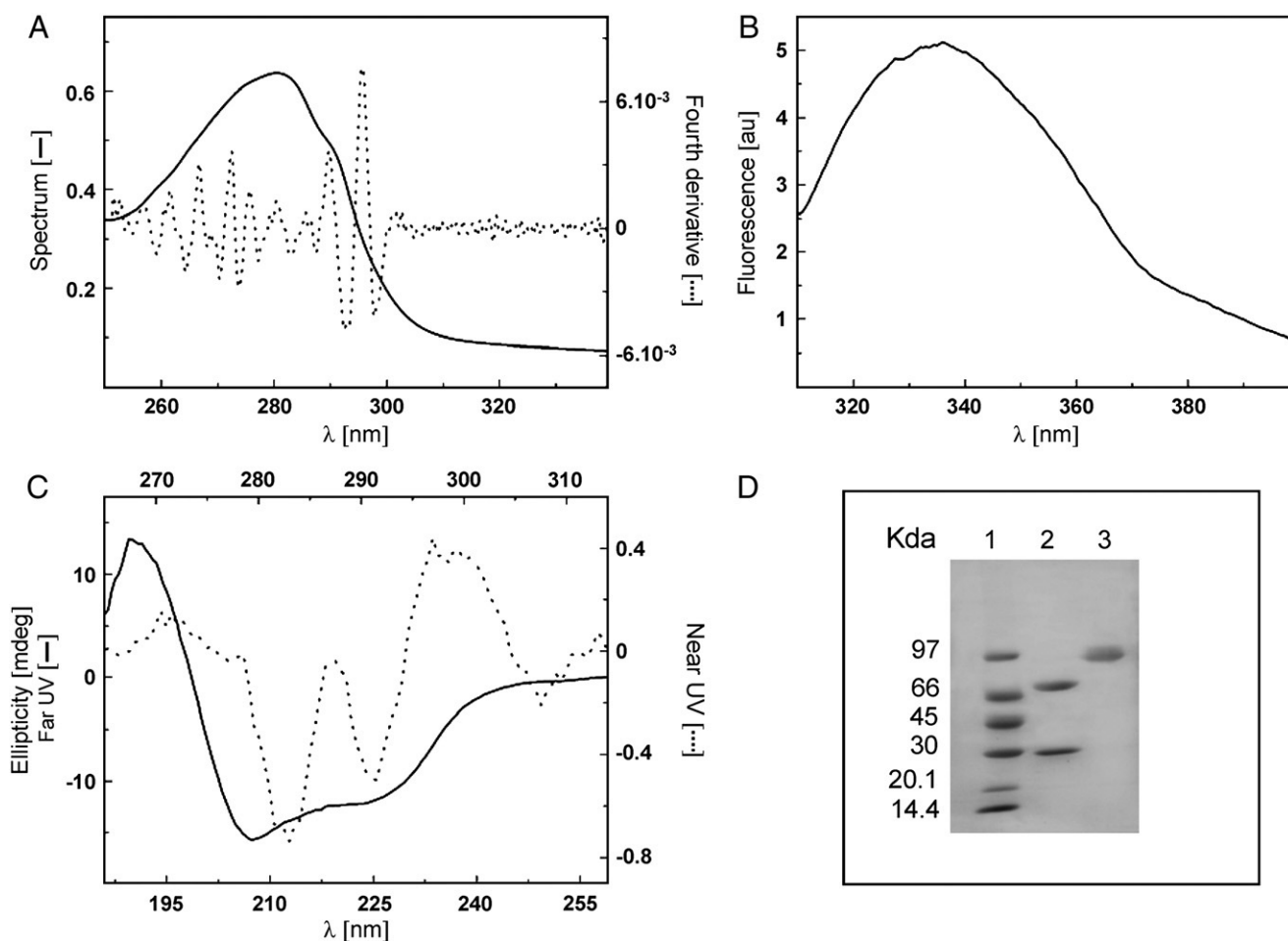


Fig. 4. Structural features of native PV2 from *P. canaliculata*. (A) Absorption spectra of PV2 (solid line), with the fourth derivative spectra (dashed line). (B) Tryptophan fluorescence spectrum of PV2. (C) CD spectra of PV2 in the near-UV region (dashed line) and far-UV region (solid line). (D) Dissociating gel electrophoresis (SDS-PAGE) was performed in 4–20% w/v polyacrylamide gradient. Lane 1: Low molecular weight standards; Lane 2: PV2 incubated with β -mercaptoethanol; Lane 3: PV2 without reducing agent.

backbone (Table 1, first line). Analysis of nCD data showed sharp spectroscopic features centered at 282 and 291 nm characteristic of buried tyrosine and tryptophan residues, respectively.

3.5. Cysteine residues

The fluorescence emission of mBrB was used to determine the number of cysteines present in PV2. The emission of mBrB displayed a clear kinetic behavior with $t_{50} = 35 \pm 1$ min. A similar experiment using BSA, produced a similar kinetic with $t_{50} = 37 \pm 1$. A comparison of the fluorescence saturation value between BSA (with

ca. 35 cysteine residues) and PV2 renders a value of 32 cysteine residues for the latter.

3.6. Fluorescence quenching experiments

To gain insight about the environment of tryptophan residues in PV2, fluorescence quenching experiments were performed by monitoring the acrylamide-induced fluorescence quenching of tryptophan emission. Increasing amounts of acrylamide scaled down the emission spectra without any noticeable blue shift as would be expected for the presence of tryptophan residues with different solvent exposure [26] (Fig. 3A). To quantify the degree of solvent exposure of the indole rings, the “sphere of action” quenching model [26,27] and Eq. (1), a modified form of the Stern-Volmer model, were

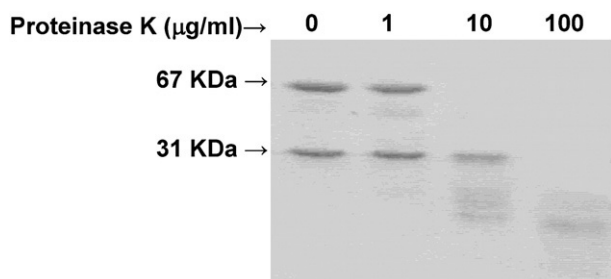


Fig. 5. Proteinase K digestion of PV2. The PV2 protein solution (0.25 mM) was incubated with the indicated concentrations of proteinase K. Products were analyzed on a SDS polyacrylamide gel (4–15%) and visualized with Coomassie blue.

Table 1
Secondary structure content of PV2 at different temperatures.

T °C	α Helix (%)		“β sheet” (%)		Rnd. coil (%)	
	K ^a	C ^b	K	C	K	C
20	21	22	22	28	56	49
60	21	15	24	38	55	47
70	9	6	43	47	48	46

^aK2d algorithm.

^bContin algorithm.

used to analyze the data. Briefly, the model postulates that inside a critical volume around the fluorophore all quenchers will have unit quenching probability. Under such assumption, the otherwise linear Stern-Volmer plot will bend up at high quencher concentrations.

$$F_0/F = (1 + K_{SV}[Q])e^{[Q]V} \quad (1)$$

$$K_{SV} = \tau_0 k_q$$

here F and F_0 correspond to the fluorescence intensity for a given quencher concentration $[Q]$ and for $[Q]=0$, respectively, K_{SV} is the Stern-Volmer quenching constant, V is the excluded volume for the quencher-fluorophore pair, τ_0 is the fluorophore excited state lifetime in absence of quencher and k_q is the apparent microscopic bimolecular quenching constant [26,27].

As expected, for high quencher concentration the probability of finding a quencher molecule within the critical sphere increases and the Stern-Volmer plot departs from the linear behavior [25,26] (see Fig. 3B). Using Eq. (1), values for $K_{SV} = 6.0 \pm 0.4 \text{ M}^{-1}$ and $V = 748 \pm 133 \text{ \AA}^3$ were obtained (full line in Fig. 3B). Assuming a spherical shape for V , a radius $r = 5.6 \pm 0.3 \text{ \AA}$ was obtained, in good agreement with the sum of the molecular radii for tryptophan and acrylamide $r_{\text{calc}} = 6.3 \text{ \AA}$ (calculated using the algorithm implemented in <http://www.molinspiration.com/cgi-bin/properties>).

Using the second line in Eq. (1) and assuming a life time $\tau_0 = 3 \text{ ns}$ for the tryptophan excited state, a value of $k_q = (2.0 \pm 0.1) \times 10^9 \text{ M}^{-1} \text{ s}^{-1}$ was obtained for the apparent bimolecular quenching constant. Regarding the value obtained for k_q and the measure λ_{max} , the wavelength for the maximum of the fluorescence spectrum, Eftink [28] described a correlation between the position of the emission maximum (λ_{max}) and the value for k_q for acrylamide quenching of tryptophan emission for single tryptophan proteins. Although a high molecular weight protein like PV2 is not likely to have a single tryptophan, our quenching experiments suggest the existence of a single class of tryptophan residues. Following Eftnik's empirical correlation it is possible to conclude that those tryptophan residues are placed in occluded, yet not totally buried, positions inside the tertiary structure of PV2.

3.7. Conformational stability

3.7.1. Urea denaturation studies

PV2 denaturation by urea was studied by solvent exposure of Trp, solvent exposure of Cys, and by changes in particle dimensions. The tryptophan fluorescence spectra obtained for PV2 at different urea concentrations is shown in Fig. 6A. Two distinctive behaviors can be observed from the spectra. At low and medium urea concentrations (up to 4.5 M), a reduction of the fluorescence intensity and a small but noticeable red shift can be observed. Above 4.5 M urea, a strong red shift and a clear increment of the fluorescence intensity were observed. The behavior at lower urea concentrations can be associated to a progressive exposure of the indole rings of the tryptophan to the polar solvent (Fig. 6A, inset). At higher urea concentrations, the removal of local interactions around tryptophans seems to release internal quenching interactions present in the native state giving rise to a noticeable increment of the fluorescence emission. The effect of the denaturant on the quaternary structure of PV2 was also followed by SAXS (Fig. 6B). The protein showed constant R_g values of $44 \pm 1 \text{ \AA}$ between 0 and 2 M urea, while for higher concentrations the gyration radii increased, reaching $66 \pm 5 \text{ \AA}$ at 6 M urea (Fig. 6B, inset). The urea induced denaturation of PV2 was finally monitored following the solvent exposure of the cysteine residues of the protein. The number of cysteine residues exposed at different urea concentrations was determined using the fluorescent emission of the probe monobromobimane (as described in precedent paragraphs). Fig. 6C shows the

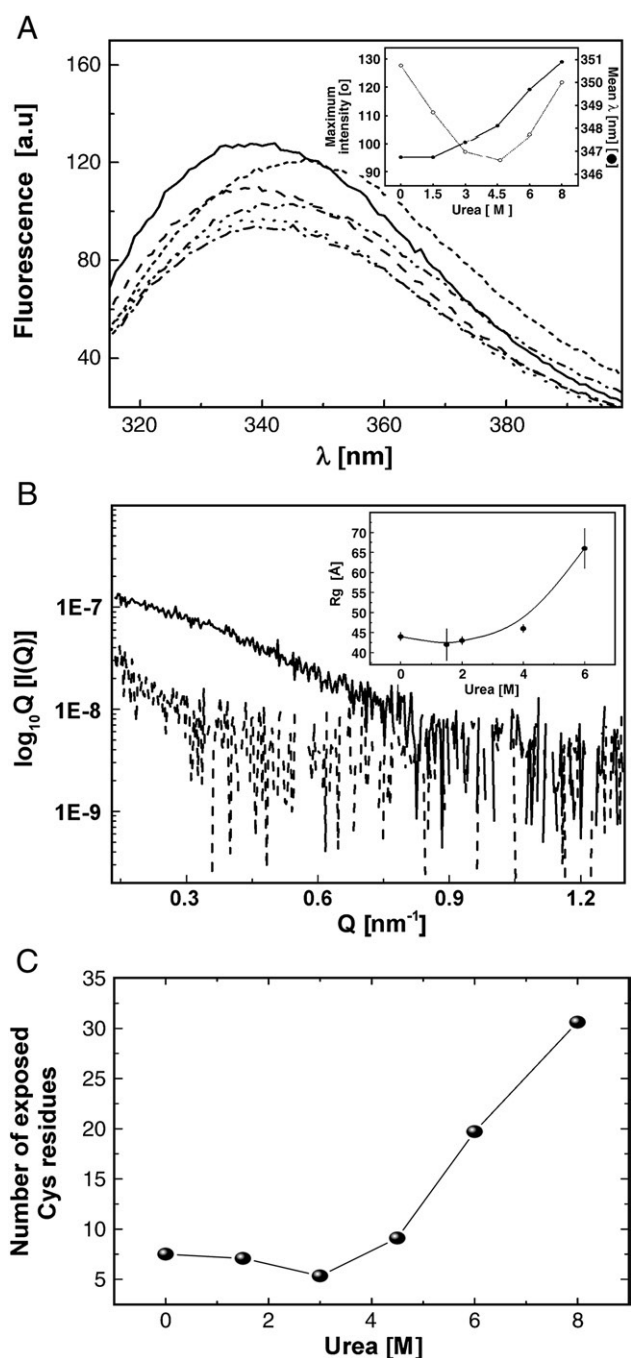


Fig. 6. PV2 unfolding induced by urea treatment. (A) Tryptophan fluorescence spectra of PV2 at 0 M (solid line), 1.5 M (dashed line), 3 M (dotted line), 4.5 M (dash dotted line), 6 M (dash dot dotted line) and 8 M (short dashed line). Inset: Mean wavelength refers to $\Sigma(\lambda F(\lambda))/\Sigma F(\lambda)$ where $F(\lambda)$ corresponds to the fluorescence intensity for a given λ (closed circle). Maximum intensity at different urea concentrations (open circle). (B) SAXS data of folded (solid line) and unfolded (dotted line) PV2. Inset: Variations of particle R_g as a function of urea concentration. (C) Number of exposed Cys residues at different urea concentration.

number of exposed cysteines at different urea concentrations indicating a dramatic increase of exposed cysteines above 4.5 M urea.

3.7.2. Thermal denaturation studies

PV2 susceptibility to temperature was studied by changes in secondary structure, exposure of trp and particle size and globularity. The fCD spectra obtained for native PV2 at different temperatures are depicted in Fig. 7A. The estimation of secondary structures (Table 1) indicated a noticeable increase in the contribution of β -sheet-like

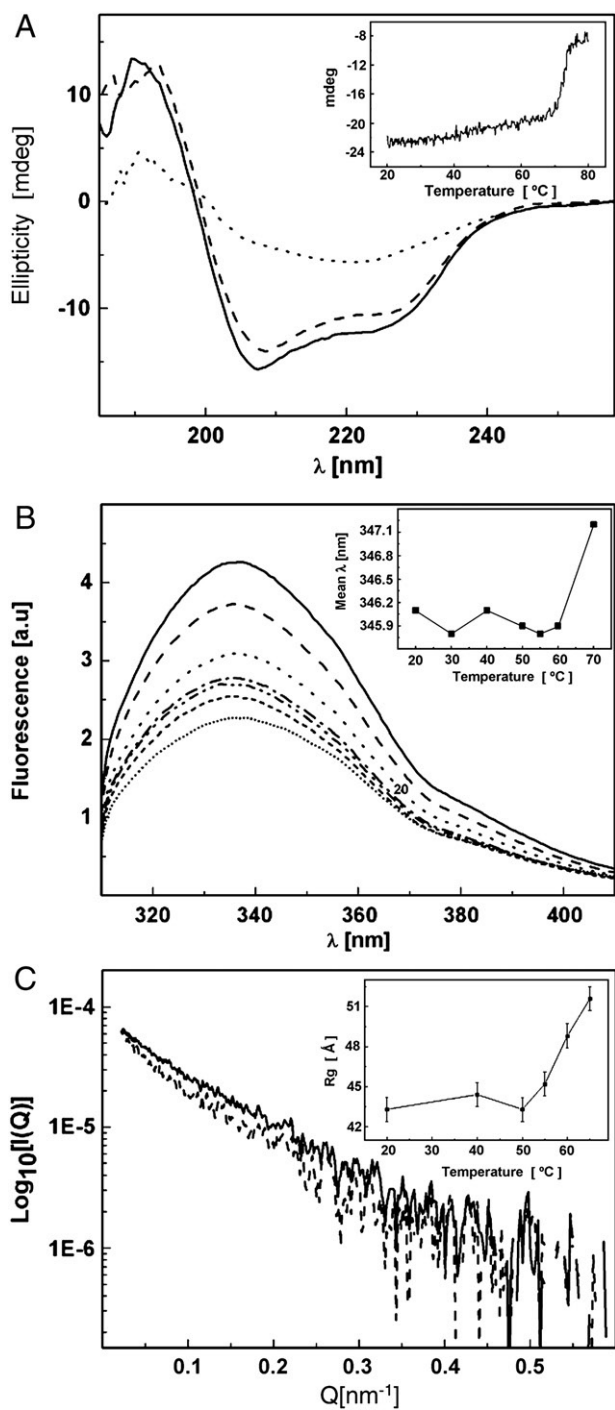


Fig. 7. Thermal-induced unfolding of native PV2. (A) Far CD spectra of PV2 at 20 °C (solid line), 60 °C (dashed line) and 70 °C (dotted line). Inset: Thermal unfolding of PV2 following the ellipticity of the CD spectra at 222 nm. (B) Tryptophan fluorescence spectra of PV2 from 20 °C (solid line) to 70 °C (dotted line). Inset: Mean wavelength refers to $\frac{\sum(\lambda F(\lambda))}{\sum F(\lambda)}$ where $F(\lambda)$ corresponds to the fluorescence intensity for a given λ . (C) Effect on size and shape as determined by SAXS at 20 °C (solid line) and 65 °C (dashed line). Inset: Variations of PV2 R_g .

structures above 60 °C.¹ When thermal stability of PV2 was followed measuring the evolution of the ellipticity at 222 nm, the protein was found to have a T_m of ~70 °C (Fig. 7A, inset). This agreed with the

¹ A possible explanation for such a behavior could be the occurrence of poly-proline like structures during unfolding that our algorithms could hardly differentiate from β structure.

fluorescence studies showing that PV2 is stable up to 60 °C. For higher temperatures, a spectral red shift and a fluorescence intensity decrease were observed indicating the exposure of tryptophan residues to the aqueous environment (Fig. 7B). Likewise, SAXS analysis of the changes in PV2 quaternary structure showed a gradual loss of globularity (reflected in the behavior of the Kratky plot) together with a simultaneous increase of the R_g to 52 ± 1 Å at 65 °C (Fig. 7C, inset).

4. Discussion

4.1. Structural features

PV2 is biochemically and functionally well characterized, but structural information was lacking. In fact, structural knowledge of invertebrate perivitellins was limited to the golden apple snail ovorubin. The possibility to obtain the PV2 oligomer in its native conformation from a natural source allowed us to perform a structural analysis using several techniques.

SAXS experiments allowed us to elaborate the first low-resolution shape model for a proteinaceous neurotoxin. The gyration radii obtained are quite compatible with the size expected for a compact oligomer of about 400 kDa, the apparent mass previously determined for PV2. TEM results were also in general agreement with the maximum pair distances obtained from SAXS results and confirmed the absence of supramolecular aggregates. A comparison of the shape with ovorubin [29], the only other perivitellin model, reported, shows similarities both being elongated particles.

The tryptophan fluorescence spectrum for native PV2 indicates that the “average” indole ring is placed in a hydrophobic environment. Acrylamide quenching results further confirm this conclusion and, surprising for a high molecular weight protein, supports the existence of a single tryptophan class with a single average quenching constant. Moreover, the Kratky plots (Iq^2 vs. q) obtained from the analysis of SAXS data suggest that the oligomer presents a compact and well folded structure in accordance with tryptophan fluorescence and CD experiments.

As a whole, these results indicate that PV2 is a compact and well folded octamer with their subunits forming 4 heterodimers, each one stabilized by intercatenary disulfide bridges, and held together by non-covalent forces. It is worth noting that additional quaternary interactions and closer packing are typical characteristics of proteins from organisms adapted to high temperatures [30].

4.2. Structural stability

Protein structural stability studies are one of the keys to understand protein function. We therefore investigated the effect of increasing temperature to induce protein denaturation, and complemented this study with the effect of a chemical denaturant to further understand the biophysical aspects of PV2 unfolding/disassembly. The thermostability study has an “added value” in this particular protein because snail eggs are exposed to high temperatures during sunlight exposure.

During urea denaturation, a red shift of the tryptophan emission spectra typical of the exposition of the indole ring to polar environments was observed. The increase in the emission intensity suggests the existence of internal quenching interactions in the native state that were gradually removed by increasing urea concentration. On the contrary, thermal-induced denaturation of PV2 gave rise to a steady decrease of the tryptophan fluorescence emission suggesting that the interaction responsible for the partial quenching of tryptophan emission in the native state cannot be removed by thermal activation. At present, no general strategies of protein stabilization have yet been established. In fact, relating the structure and stability of homologous proteins from mesophiles and extremophiles, it becomes clear that stability increment may accumulate from local interactions, secondary

or supersecondary structure, packing and docking of domains, association of subunits, and conjugation with prosthetic groups such as carbohydrates [31,32]. PV2 stability seems to fall into this general adaptative strategy. Interestingly, chemical and thermal structural perturbations induced a size expansion of the quaternary structure of PV2 instead of the expected decrease caused by the disassembling of the oligomer. This is compatible with the unfolding of the heterodimers but without disassembling probably due to the intercatenary disulfide bridges identified between their subunits. Both ovorubin, PV2 perivitellins display a high thermal stability above 60–70 °C, suggesting an adaptative mechanism to the challenging environmental conditions that *P. canaliculata* eggs must withstand during development [11] and highlighting the physiological significance of perivitellins in the reproductive biology of these molluscs.

Acknowledgments

M.S.D. is member of Carrera del Investigador CICBA, Argentina. H.H. and M.C. are members of Carrera del Investigador CONICET, Argentina. V.F. is a doctoral fellow, CONICET, Argentina. M.C. and H.H. are full professors in Universidad Nacional del Noroeste de Buenos Aires, Pergamino, and Universidad Nacional de La Plata, Argentina, respectively. This work was supported by CONICET (PIP No. 5888), ANPCyT (PICT No. 2166), and by partial financial support from LNLS - Brazilian Synchrotron Light Laboratory/MCT (Projects D11A-SAXS1-5207/06 and 5267). We also thank LNLS - Brazilian Synchrotron Light Laboratory/MCT for access to their facilities. We thank Dr. M. Ermácora for kindly providing access to the CD equipment.

Appendix A. Supplementary data

Supplementary data associated with this article can be found, in the online version, at [doi:10.1016/j.bbapap.2010.02.013](https://doi.org/10.1016/j.bbapap.2010.02.013).

References

- [1] E.A. Albrecht, N.B. Carreño, A. Castro-Vazquez, A quantitative study of environmental factors influencing the seasonal onset of reproductive behaviour in the south American apple-snail *Pomacea canaliculata* (Gastropoda: Ampullariidae), *J. Mollus. Stud.* 65 (1999) 241–250.
- [2] E.A. Albrecht, E. Koch, N.B. Carreño, A. Castro-Vazquez, Control of the seasonal arrest of copulation and spawning in the apple snail *Pomacea canaliculata* (Prosobranchia: Ampullariidae): differential effects of food availability, water temperature, and day length, *Veliger* 47 (2004) 169–174.
- [3] N.V. Pizani, A.L. Estebenet, P.R. Martín, Effects of submersion and aerial exposure on clutches and hatchlings of *Pomacea canaliculata* (Gastropoda: Ampullariidae), *Am. Malacol. Bull.* 20 (2005) 55–63.
- [4] H. Heras, C.F. Garín, R.J. Pollero, Biochemical composition and energy sources during embryo development and in early juveniles of the snail *Pomacea canaliculata* (Mollusca: Gastropoda), *J. Exp. Zool.* 280 (1998) 375–383.
- [5] H. Heras, M.S. Dreon, S. Ituarte, R.J. Pollero, Egg carotenoproteins in neotropical Ampullariidae (Gastropoda: Arquitaenioglossa), *Comp. Biochem. Physiol. C* 146 (2007) 158–167.
- [6] C.F. Garín, H. Heras, R.J. Pollero, Lipoproteins of the egg perivitellin fluid of *Pomacea canaliculata* snails (Mollusca: Gastropoda), *J. Exp. Zool.* 276 (1996) 307–314.
- [7] C.P. Raven, Chemical Embriology of Mollusca, in: M. Florin, B.T. Scheer (Eds.), *Chemical Zoology*, Academic Press, New York, 1972, pp. 155–185.
- [8] M.S. Dreon, G. Schinella, H. Heras, R.J. Pollero, Antioxidant defense system in the apple snail eggs, the role of ovorubin, *Arch. Biochem. Biophys.* 422 (2004) 1–8.
- [9] M.S. Dreon, H. Heras, R.J. Pollero, Biochemical composition, tissue origin and functional properties of egg perivitellins from *Pomacea canaliculata*, *Biocell* 30 (2006) 359–365.
- [10] M.S. Dreon, H. Heras, R.J. Pollero, Characterization of the major egg glycolipoproteins from the perivitellin fluid of the apple snail *Pomacea canaliculata*, *Mol. Reprod. Dev.* 68 (2004) 359–364.
- [11] M.S. Dreon, M. Ceolín, H. Heras, Astaxanthin binding and structural stability of the apple snail carotenoprotein ovorubin, *Arch. Biochem. Biophys.* 460 (2007) 107–112.
- [12] S. Ituarte, M.S. Dreon, R.J. Pollero, H. Heras, Isolation and partial characterization of a new lipo-glyco-carotenoprotein from *Pomacea scalaris* (Gastropoda: Ampullariidae), *Mol. Reprod. Dev.* 75 (2008) 1441–1448.
- [13] H. Heras, M.V. Frassa, P.E. Fernández, C.M. Galosi, E.J. Gimeno, M.S. Dreon, First egg protein with a neurotoxic effect on mice, *Toxicol.* 52 (2008) 481–488.
- [14] V.B. Gerritsen, A snail's sting, *Protein Spotlight* 100 (2008) 1–2.
- [15] O.H. Lowry, N.J. Rosenbrough, A.L. Farr, R. Randall, Protein measurement with the Folin phenol reagent, *J. Biol. Chem.* 193 (1951) 265–275.
- [16] W.H. Press, B.P. Flannery, S.A. Teukolsky, W.T. Vetterling, *Numerical Recipes: The Art of Scientific Computing*, Cambridge University Press, Cambridge, USA, 1988.
- [17] M. Knocker, I. Dol, Effects of noise in derivative spectrophotometry: anomalous bias arising from amplitude measurements, *Analyst* 117 (1992) 1385–1397.
- [18] U.K. Laemmli, Cleavage of structural proteins during the assembly of the head of bacteriophage T4, *Nature* 227 (1970) 680–685.
- [19] E.M. Kosower, N.S. Kosower, Bromobimane probes for thiols, *Methods Enzymol.* 251 (1995) 133–148.
- [20] M.A. Andrade, P. Chacón, J.J. Merelo, F. Morán, Evaluation of secondary structure of proteins from UV circular dichroism using an unsupervised learning neural network, *Prot. Eng.* 6 (1993) 383–390.
- [21] S.W. Provencher, J. Glockner, Estimation of globular protein secondary structure from circular dichroism, *Biochemistry* 20 (1981) 33–37.
- [22] D.I. Svergun, Restoring low resolution structure of biological macromolecules from solution scattering using simulated annealing, *Biophys. J.* 76 (1999) 2879–2886.
- [23] D.I. Svergun, GNOM 4.5, *J. Appl. Cryst.* 25 (1992) 495–503.
- [24] V.V. Volkov, D.I. Svergun, Uniqueness of ab initio shape determination in small-angle scattering, *J. Appl. Cryst.* 36 (2003) 860–864.
- [25] D.I. Svergun, Determination of the regularization parameter in indirect-transform methods using perceptual criteria, *J. Appl. Crystallog.* 25 (1992) 495–503.
- [26] J.R. Lakowicz, *Principles of Fluorescence Spectroscopy*, Kluwer Academic / Plenum Publishers, New York, 1999.
- [27] I.M. Frank, S.L. Vavilov, Über Die Wirkungssphäre Der Auslöschungs-Fargänge in Den Fluoreszierenden Flüssigkeiten, 1931, pp. 100–110.
- [28] M.R. Eftink, *Fluorescence Spectroscopy, Vol. 2, Principles*, Plenum Press, New York, 1991.
- [29] D.F. Cheesman, Ovourubin, a chromoprotein from the eggs of the gastropod mollusk *Pomacea canaliculata*, *Proc. R. Soc. Lond. [Biol.]* 149 (1958) 571–587.
- [30] R. Jaenicke, Stability and stabilization of globular proteins in solution, *J. Biotechnol.* 79 (2000) 193–203.
- [31] R. Jaenicke, How do proteins acquire their three-dimensional structure and stability? *Naturwissenschaften* 83 (1996) 544–554.
- [32] R. Jaenicke, Stability and folding of ultrastructural proteins: eye lens crystallins and enzymes from thermophiles, *FASEB J.* 10 (1996) 84–92.